Geometrical interpretation of the argument of weak values of general observables in N-level quantum systems

Ballesteros Ferraz, Lorena; Lambert, Dominique L.; Caudano, Yves

Published in:
Quantum Science and Technology

DOI:
10.1088/2058-9565/ac8bf1

Publication date:
2022

Document Version
Peer reviewed version

Geometrical interpretation of the argument of Bargmann invariants and weak values in N-level quantum systems applying the Majorana symmetric representation

Lorena B Ferraz[1], Dominique L Lambert[2] and Yves Caudano[1]
[1] *Research Unit Lasers and Spectroscopies (UR-LLS), naXys & NISM, University of Namur, Rue de Bruxelles 61, B-5000 Namur, Belgium* and*
[2] *ESPHIN & naXys, University of Namur, Rue de Bruxelles 61, B-5000 Namur, Belgium*

In this paper, we study the argument of weak values of general observables, succeeding to give a geometric description to this argument on the Bloch sphere. We apply the Majorana symmetric representation to reach this goal. The weak value of a general observable is proportional to the weak value of an effective projector: it arises from the normalized application of the observable over the initial state, with a constant of proportionality that is real. The argument of the weak value of a projector on a pure state of an N-level system corresponds to a symplectic area in the complex projective space (CP^{N-1}), which can be represented geometrically with a sum of $N-1$ solid angles on the Bloch sphere using the Majorana stellar representation. Here, we show that the argument of the weak value of a general observable can be described, using Majorana representation, as the sum of $N-1$ solid angles on the Bloch sphere, merging both studies. These two approaches provide two geometrical descriptions, a first one in CP^{N-1} and a second one on the Bloch sphere, after mapping the problem from the original space (CP^{N-1}) by making use of the Majorana representation. These results can also be applied to the argument of the third-order Bargmann invariant, the most fundamental order as the argument of any higher order invariant can be expressed as a sum of the argument of third-order Bargmann invariants. Finally, we focus on the argument of the weak value of a general spin-1 operator when its modulus diverges towards infinity. This divergence amplifies signals with great usefulness in experiments.

INTRODUCTION

Weak values have a great potential, and several applications in different areas of quantum physics rely on them due to both their fundamental and experimental properties[1–3].

Weak values arise notably when performing weakly a measurement of an observable through a unitary operator, followed by post-selection (executing a projective measurement and filtering the final state). Aharanov defined this quantity in the context of the von Neumann scheme [4, 5]. In this protocol, the global system is composed by the measuring device (or ancilla) and the system of interest. The system and the ancilla interact through a unitary operator, $\hat{U} = \exp\left\{-ig\hat{A}\otimes\hat{P}\right\}$, where $\hat{A}$, belonging to the system space, is the operator to be measured and $\hat{P}$, representing the momentum operator, belongs to the measuring device space. After this interaction, the wave function of the probe becomes a linear combination of wave functions that are shifted by quantities proportional to each of the eigenvalues of the observable [6, 7]. When the interaction strength, g, is small, the measurement is weak, and the average shift in the ancilla's wave function is proportional to the expectation value of the observable $\hat{A}$. Nonetheless, when post-selection is executed on the system after the measurement, all shifted wave functions are projected on a common state and thus interfere. As a result, the measuring device's wave function is typically shifted in position by a quantity proportional to the real part of the weak value $A_w = \frac{\langle\psi_f|\hat{A}|\psi_i\rangle}{\langle\psi_f|\psi_i\rangle}$, where $|\psi_i\rangle$ and $|\psi_f\rangle$ are the pre- and post-selected states. The ancilla's wave function is simultaneously shifted in momentum by a quantity that is proportional to the imaginary part of the weak value [6, 7].

Several schemes extended the weak measurement protocol beyond the specific configuration in which they were defined [5]. The pointer can be any observable in continuous or discrete space. Furthermore, any observable can play the role of the probe, but the resulting shift is a linear combination of the real and imaginary parts [6]. Additionally, weak values can arise in more general schemes than weak measurements, for example, without a probe [8, 9] or in strong measurements [10].

Applications of weak measurements abound in different areas. Weak values are unbounded numbers; they enhance tiny signals [11–13] and hence are a useful tool for sensing [14–16]. As complex numbers, they can be used in tomography [17–21], for measuring wave functions [21] and for measuring the expectation value of non-Hermitian operators [22]. They also present a great potential in quantum computing [23].

Scientists usually study weak values in terms of their real and imaginary parts [7]. Nonetheless, to provide a geometrical interpretation of these quantities, which has taken much attention over the last few years [24–30], it is essential to investigate the argument. Anomalous weak values (complex values or values outside of the range of the possible expectation values of the observable) are proofs of contextuality, essential property for the supremacy of quantum computing [2, 31]. The argument

of the weak value can thus help us to understand the controversial meaning of weak values. From a practical point of view, the argument provides the direction in which the coherent state of a Gaussian meter is shifted in phase space after post-selection in a weak measurement. Moreover, the real part of weak values is linked to the optimal conditional estimate of the observable, while the imaginary part is related to the inaccuracy of the estimate [32–35]. In consequence, the argument appears connected to a ratio of the estimate and its contribution to the error. In general, studying the geometric phase arising from weak values can benefit the study of interferometric phenomena with post-selection.

The argument of the weak value of two-level projectors is associated to a geometric phase that is proportional to the solid angle on the Bloch sphere of the spherical triangle spanned by the pre-selected state, the projector state and the post-selected state [36]. Recently, it has been shown that for N-level systems, the argument of the weak value of a projector represents a geometric phase associated to the symplectic area of the geodesic triangle spanned by the pre-selected state, the projector state, and the post-selected state in CP^{N-1} [37]. As the argument of the weak value of any observable is equivalent to the argument of the weak value of an effective projector (an extra phase is involved, with 0 or π as sole possible values), we can apply the geometric description previously developed for projectors to weak values of general observables.

Cormann et al showed that the argument of the weak value of N-level projectors can be expressed as the sum of $N-1$ solid angles on the Bloch sphere. For this, they applied Majorana representation to the three states (initial state, projector state, and post-selected state)[26]. Majorana introduced in the 1930s a mathematical procedure to represent systems larger than qubits on the Bloch sphere. $N-1$ stars on the Bloch sphere represent an N-level system [38]. The Majorana representation is a powerful tool to get a geometrical insight and to perform calculations [39–41]. Several studies, from purely theoretical to quantum computing, made use of this representation [42–44].

Visualizing a symplectic area in CP^{N-1} is not an intuitive task, as it is not the usual Riemannian area. To tackle this problem, in this paper, we show that, by applying the Majorana representation to the three states involved in the weak value of any N-level observable (pre-selected state, effective projector state [37], and post-selected state), the geometry of the full system is brought to the Bloch sphere. The argument of the weak value is the sum of $N-1$ solid angles on the Bloch sphere. The argument of the projector weak value is equivalent to the argument of the Bargmann invariant associated to the three states (invariant under gauge transformation and re-parametrization). The geometric interpretation is thus also appropriate in this context. Bargmann invariants are directly linked to the Kirkwood-Dirac pseudo-probability that defines a non-classical state by taking negative or complex values [45]. Third-order Bargmann invariants, $\mathrm{Tr}\left(\hat{\Pi}_1\hat{\Pi}_2\hat{\Pi}_3\right)$, are especially interesting, as the argument of any N-order Bargmann, $\mathrm{Tr}\left(\hat{\Pi}_1\hat{\Pi}_2\ldots\hat{\Pi}_N\right)$ can be expressed as the sum of $N-2$ arguments of third-order Bargmann invariants [46]. The weak value is equal to a third-order Bargmann invariant divided by the projection probability of the pre- and post-selected states.

This paper is structured as follows. In the first section, we present the geometric interpretation of weak values of N-level general observables, by applying the Majorana representation. In section II, these calculations are applied to the specific case of 3-level systems. After this, we present the relevant example of spin-1 systems: we study the argument of the weak value of a spin-1 operator when the modulus of the weak value presents a divergence, a typical situation of an amplification effect appearing in a weak measurement with nearly orthogonal pre- and post-selected states.

WEAK VALUES OF N-LEVEL OBSERVABLES IN TERMS OF MAJORANA STARS

The initial state, the observable and the post-selected state constitute the required components of a weak value. Varying any of these parts can completely modify the quantity. In this section, we provide the theoretical framework to apply the Majorana representation to the different components of the weak value of an N-level observable.

The weak value of any discrete observable is proportional to the weak value of a very specific projector with a constant of proportionality that is real [37],

$$A_w = \frac{\langle\psi_f|\,\hat{A}\,|\psi_i\rangle}{\langle\psi_f|\psi_i\rangle} = \frac{\langle\psi_i|\,\hat{A}^2\,|\psi_i\rangle}{\langle\psi_i|\,\hat{A}\,|\psi_i\rangle}\frac{\langle\psi_f|\,\hat{\Pi}_{i'}\,|\psi_i\rangle}{\langle\psi_f|\psi_i\rangle}, \qquad (1)$$

where $\hat{\Pi}_{i'} = |\psi_{i'}\rangle\langle\psi_{i'}|$, with,

$$|\psi_{i'}\rangle = \frac{1}{\sqrt{\langle\psi_i|\,\hat{A}^2\,|\psi_i\rangle}}\hat{A}\,|\psi_i\rangle\,, \qquad (2)$$

Eq.(1) does not present any issue of definition. When $\langle\hat{A}^2\rangle_{\psi_i} = 0$, the weak value A_w is equal to 0. If the expectation value of $\hat{A}$ in the initial states is equal to 0, then the weak value of the effective projector is calculated through a limit, using a small parameter ϵ that tends to 0 (for more detail, see [37]).

As the weak value is invariant under unitary transformations, two unitary operators are applied to take

two states to separable states in the Majorana representation. It is always possible to map two states to separable states (degenerate stars, i.e. a coherent state) in the Majorana representation [47]. The pre-selected state is mapped to $|\psi_i\rangle \rightarrow |\Psi_i'\rangle = \underbrace{|0\rangle ... |0\rangle}_{N-1}$ via applying an appropriate unitary operator $\hat{U}^{(1)}$. The general form of the unitary operator to take a state $|\psi_1\rangle$ to another state $|\psi_2\rangle$ is $\hat{U} = e^{-i\arg\langle\psi_2|\psi_1\rangle}\left(\hat{I} - 2\,|\Delta\rangle\langle\Delta|\right)$, where $|\Delta\rangle = \frac{e^{-i\arg\langle\psi_2|\psi_1\rangle}|\psi_1\rangle - |\psi_2\rangle}{\sqrt{2(1-|\langle\psi_2|\psi_1\rangle|)}}$. The other components are also affected by the unitary transformation, $\hat{A} \rightarrow \hat{U}^{(1)}\hat{A}\hat{U}^{(1)^\dagger} = \hat{A}'$, and $\hat{U}^{(1)}|\psi_f\rangle = \left|\psi_f'\right\rangle$. A second unitary operator $\hat{U}^{(2)}$ that leaves the pre-selected state invariant, $|\psi_i''\rangle = \hat{U}^{(2)}|\psi_i'\rangle = |\psi_i'\rangle$, is applied to map the state $|\psi_{i'}\rangle$ to a second separable state, $|\psi_{i'}'\rangle \rightarrow |\Psi_{i'}''\rangle = \underbrace{|\phi_{i'}\rangle ... |\phi_{i'}\rangle}_{N-1}$. This unitary operator should also be applied to the post-selected state, $\hat{U}^{(2)}\left|\psi_f'\right\rangle = \left|\psi_f''\right\rangle$.

After both unitary operators, the post-selected state becomes a general N-level state, $\left|\Psi_f''\right\rangle = \frac{1}{\sqrt{M}}\sum_P \hat{P}\left[\left|\phi_f^{(1)}\right\rangle ... \left|\phi_f^{(N-1)}\right\rangle\right]$, where the sum runs through all the permutations. After removing the global phase [48], the state can be written as a symmetric state in the Majorana representation. Writing the state as $\left|\psi_f''\right\rangle = \sum_{i=0}^{N-1} c_i\,|i\rangle$ and solving the Majorana polynomial, Eq.(3), one can express the state in the Majorana symmetric representation [49, 50],

$$P(z) = \sum_{k=0}^{N-1} (-1)^k \sqrt{C_{N-1}^k}\, c_k z^{N-1-k}, \tag{3}$$

where the binomial coefficients $C_k^{N-1} = \frac{(N-1)!}{k!(N-1-k)!}$ and c_k are the coefficients of the state $\left|\psi_f''\right\rangle$. The polar, θ_k, and azimuthal, ϕ_k, angles on the Bloch sphere depend respectively on the modulus and the phase of the roots z_k of the polynomial Eq.(3),

$$z_k = e^{j\phi_k}\tan\frac{\theta_k}{2}, \tag{4}$$

where $0 \leq \phi_k \leq 2\pi$, and $0 \leq \theta_k \leq \pi$.

The weak value is now calculated, following Eq.(1), as,

$$A_w = \frac{\left\langle\psi_f''\right|\hat{A}''\left|\psi_i''\right\rangle}{\left\langle\psi_f''\middle|\psi_i''\right\rangle} = \frac{\langle\psi_i|\hat{A}^2|\psi_i\rangle}{\langle\psi_i|\hat{A}|\psi_i\rangle}\Pi_{i',w}^{(1)}\Pi_{i',w}^{(2)}\ldots\Pi_{i',w}^{(N-1)}, \tag{5}$$

where each two-level system weak value is $\Pi_{i',w}^{(j)} = \frac{\left\langle\phi_f^{(j)}\middle|\phi_{i'}\right\rangle\langle\phi_{i'}|\phi_i\rangle}{\left\langle\phi_f^{(j)}\middle|\phi_i\right\rangle}$.

The modulus of the weak value is thus the product of $N-1$ moduli of weak values of qubit projectors,

$$\begin{aligned}|A_w| &= \frac{\langle\psi_i|\hat{A}^2|\psi_i\rangle}{|\langle\psi_i|\hat{A}|\psi_i\rangle|}|\Pi_{i',w}^{(1)}|\cdot|\Pi_{i',w}^{(2)}|...|\Pi_{i',w}^{(N-1)}| \qquad (6)\\ &= \langle\psi_i|\hat{A}^2|\psi_i\rangle\left|\frac{\left\langle\phi_f^{(1)}\middle|\phi_{i'}\right\rangle}{\left\langle\phi_f^{(1)}\middle|\phi_i\right\rangle}\right|\left|\frac{\left\langle\phi_f^{(2)}\middle|\phi_{i'}\right\rangle}{\left\langle\phi_f^{(2)}\middle|\phi_i\right\rangle}\right|\ldots\left|\frac{\left\langle\phi_f^{(N-1)}\middle|\phi_{i'}\right\rangle}{\left\langle\phi_f^{(N-1)}\middle|\phi_i\right\rangle}\right|\end{aligned}$$

The argument of the weak value of $\hat{A}$ is the sum of $N-1$ arguments of weak values of qubit projectors and the argument of the expected value of the operator $<\hat{A}>_i$, which is either 0 or π.

$$\begin{aligned}&\arg A_w = \qquad (7)\\ &= \arg\Pi_{i',w}^{(1)} + \arg\Pi_{i',w}^{(2)} + ... + \arg\Pi_{i',w}^{(N-1)} - \arg<\hat{A}>_i,\\ &= -\frac{\Omega_{ii_1'f}}{2} - \frac{\Omega_{ii_2'f}}{2} - ... - \frac{\Omega_{ii_{N-1}'f}}{2} - \arg<\hat{A}>_i\\ &= \sum_j \arg\left(\left\langle\phi_i\middle|\phi_f^{(j)}\right\rangle\left\langle\phi_f^{(j)}\middle|\phi_{i'}\right\rangle\right) - \arg<\hat{A}>_i\end{aligned}$$

Each argument of a qubit projector weak value represents a geometric phase that is associated with the area of the solid angle on the Bloch sphere of the spherical triangle spanned by the vectors representing the pre-selected state, the application of the observable over the initial state and the post-selected state in the Majorana representation.

The argument of the weak value of an observable in N-level system represents a geometric phase that is associated to the symplectic area of the geodesic triangle spanned by the geodesics linking the three vectors representing the pre-selected state, the application of the observable over the pre-selected state and the post-selected state in CP^{N-1}. This space is a Kähler manifold, which means that there are three compatible structures: the complex structure, the symplectic structure and the Riemannian structure. In CP^1, the symplectic area and the Riemannian one coincide. Hence, the argument of the weak value of an observable in two-level systems can be described in terms of solid angles. Using Majorana's description, we succeed to associate a symplectic area in CP^{N-1} with $N-1$ solid angles on the Bloch sphere. However, the spherical triangle associated to the solid angles, Ω, are not geodesic curves of CP^{N-1} in the Majorana representation.

MAJORANA REPRESENTATION OF WEAK VALUES OF OBSERVABLES IN THREE-LEVEL SYSTEMS

In this section, we focus on general weak values of three-level general observables, $\hat{A} = a_I\hat{I} + a_L\vec{\alpha}\cdot\vec{\hat{\lambda}}$, where

$\vec{\hat{\lambda}}$ are the Gell-Mann matrices (Appendix 1). Three-level systems are specially relevant. On the one hand, there are several interesting observables in three-level systems, such as the spin-1 operators, the 3D Stokes parameter operators, or three-level projectors like those appearing in the three-box paradox [51–54]. On the other hand, as weak values are only dependent on three vectors, the description of a single weak value is intrinsically a three-level problem. As weak values are invariant under unitary transformations, it is feasible to apply three unitary operators to transform the three N-level vectors into three states with only three components different from zero. In practice, this maps the vectors and their associated geodesic triangles to a three-dimensional subspace of CP^{N-1}, equivalent to CP^2. By applying this procedure, any weak value of systems larger than three dimensions can be converted to a three-level weak value, providing a representation of its argument of the weak value as two solid angles on the Bloch sphere. Consequently, we can always choose to represent the argument with $N-1$ or two solid angles.

Any projector of a pure three-level state can be written in terms of the Gell-Mann matrices and the identity as $\hat{\Pi}_a = \frac{1}{3}\left(\hat{I} + \sqrt{3}\vec{a}\cdot\vec{\hat{\lambda}}\right)$. The weak value of $\hat{A}$ is $A_w = \frac{\langle\psi_f|\hat{A}|\psi_i\rangle}{\langle\psi_f|\psi_i\rangle} = \frac{\mathrm{Tr}\left[\hat{\Pi}_f\hat{A}\hat{\Pi}_i\right]}{\mathrm{Tr}\left[\hat{\Pi}_f\hat{\Pi}_i\right]}$, which is proportional to the weak value of the projector $\hat{\Pi}_{i'}$, where $|\psi_{i'}\rangle$ is defined in Eq.(2). Owing to this property, the weak values of general observables are directly linked to Bargmann invariants. The argument of the weak value is equal to the argument of a Bargmann invariant up to a phase of either 0 or π.

Having a description of weak values of general observables in terms of projectors, the Majorana representation can be applied to all three states. In that case, the system is mapped from CP^2 to a representation on the Bloch sphere. The argument of the weak value of a projector is the sum of the arguments of two weak values in two-level systems. Each of these arguments is associated to a solid angle on the Bloch sphere.

Let's consider a general pre-selected state $|\psi_i\rangle$ in CP^2 (removing the global phase),

$$|\psi_i\rangle = \left(\cos\theta_i, e^{j\chi_{1i}}\cos\epsilon_i\sin\theta_i, e^{j\chi_{2i}}\sin\epsilon_i\sin\theta_i\right)^T, \quad (8)$$

where j is the complex unit. As the weak value is invariant under unitary transformations, we choose to map the pre-selected state to the state $|\psi_i'\rangle = (1,0,0)^T$ that is separable in the Majorana representation, $|\Psi_i'\rangle = |\phi_i\rangle|\phi_i\rangle$, $|\phi_i\rangle = |0\rangle$, choosing $|0\rangle = (1,0)^T$ and $|1\rangle = (0,1)^T$. The unitary operator that maps the pre-selected state to the state $|\psi_i'\rangle$ is,

$$\hat{U}^{(1)} = \begin{pmatrix} \cos\theta_i & e^{-j\chi_{1i}}\cos\epsilon_i\sin\theta_i & e^{-j\chi_{2i}}\sin\epsilon_i\sin\theta_i \\ \sin\theta_i & -e^{-j\chi_{1i}}\cos\epsilon_i\cos\theta_i & -e^{-j\chi_{2i}}\sin\epsilon_i\cos\theta_i \\ 0 & -e^{-j\chi_{1i}}\sin\epsilon_i & e^{-j\chi_{2i}}\cos\epsilon_i \end{pmatrix} \quad (9)$$

When applying this unitary operator to the system, the post-selected state and the observable are also modified, $|\psi_f\rangle \rightarrow \left|\psi_f'\right\rangle$ and $\hat{A} \rightarrow \hat{A}'$. After removing the phase on the first component of the state [55] arising from the application of the observable over the initial state, $|\psi_{i'}'\rangle$ can be written as $|\psi_{i'}'\rangle = \left(\cos\theta_{i'}, e^{j\chi_{1i'}}\cos\epsilon_{i'}\sin\theta_{i'}, e^{j\chi_{2i'}}\sin\epsilon_{i'}\sin\theta_{i'}\right)^T$. At this stage, we apply a second unitary operator $\hat{U}^{(2)}$ that leaves $|\psi_i'\rangle$ invariant and takes the state $|\psi_{i'}'\rangle$ to a separable state,

$$\hat{U}^{(2)} = \begin{pmatrix} 1 & 0 & 0 \\ 0 & e^{-j\chi_{1i'}}\cos\alpha & -e^{-j\chi_{2i'}}\sin\alpha \\ 0 & e^{-j\chi_{1i'}}\sin\alpha & e^{-j\chi_{2i'}}\cos\alpha \end{pmatrix}, \quad (10)$$

where $\alpha = -\epsilon_{i'} + \arcsin\left(\tan\frac{\theta_{i'}}{2}\right)$. This unitary transformation maps $|\psi_{i'}'\rangle$ to $|\psi_{i'}''\rangle = \left(\cos\theta_{i'}, \sqrt{2\cos\theta_{i'}\left(1-\cos\theta_{i'}\right)}, 1-\cos\theta_{i'}\right)^T$ which, in terms of qubits, is $|\Psi_{i'}''\rangle = |\phi_{i'}\rangle|\phi_{i'}\rangle$, with $|\phi_{i'}\rangle = \left(\sqrt{\cos\theta_{i'}}, \sqrt{1-\cos\theta_{i'}}\right)^T$.

After applying both unitary transformations ($\hat{U}^{(1)}$ and $\hat{U}^{(2)}$), the post-selected state $\left|\psi_f''\right\rangle$ has the general form, $\left|\psi_f''\right\rangle = c_0|0\rangle + c_1|1\rangle + c_2|2\rangle$. To obtain the Majorana symmetrized state, one should solve the following polynomial [47],

$$c_2 - \sqrt{2}c_1 z + c_0 z^2 = 0 \quad (11)$$

The polar, θ_k, and azimuthal, ϕ_k, angles on the Bloch sphere can be calculated from the roots z_k of the polynomial, Eq.(11).

Once all the transformations are applied, the three states are easily mapped to the Bloch sphere,

$$\begin{aligned} &|\psi_i\rangle \rightarrow |\Psi_i\rangle = |0\rangle|0\rangle \\ &|\psi_{i'}\rangle \rightarrow |\Psi_{i'}\rangle = |\phi_{i'}\rangle|\phi_{i'}\rangle \\ &|\psi_f\rangle \rightarrow |\Psi_f\rangle = \frac{1}{\sqrt{M}}\left(\left|\phi_f^{(1)}\right\rangle\left|\phi_f^{(2)}\right\rangle + \left|\phi_f^{(2)}\right\rangle\left|\phi_f^{(1)}\right\rangle\right), \end{aligned} \quad (12)$$

with $M = 2\left(1 + |\left\langle\phi_f^{(1)}\middle|\phi_f^{(2)}\right\rangle|^2\right)$. The weak value written in terms of the new states is,

$$\begin{aligned} A_w &= \frac{\langle\psi_i|\hat{A}^2|\psi_i\rangle}{\langle\psi_i|\hat{A}|\psi_i\rangle}\frac{\left\langle\phi_f^{(1)}\middle|\phi_{i'}\right\rangle\left\langle\phi_f^{(2)}\middle|\phi_{i'}\right\rangle\langle\phi_{i'}|\phi_i\rangle^2}{\left\langle\phi_f^{(1)}\middle|\phi_i\right\rangle\left\langle\phi_f^{(2)}\middle|\phi_i\right\rangle} \\ &= \frac{\langle\psi_i|\hat{A}^2|\psi_i\rangle}{\langle\psi_i|\hat{A}|\psi_i\rangle}\Pi_{i',w}^{(1)}\Pi_{i',w}^{(2)}, \end{aligned} \quad (13)$$

where $\Pi_{i',w}^{(n)} = \frac{\langle\phi_f^n|\phi_{i'}\rangle\langle\phi_{i'}|\phi_i\rangle}{\langle\phi_f^n|\phi_i\rangle}$. The quantity $\langle\psi_i|\hat{A}^2|\psi_i\rangle$ is real and positive and $\langle\psi_i|\hat{A}|\psi_i\rangle$ is real, therefore, the argument of the weak value is the sum of the arguments of both weak values and an extra phase that is either 0

or π,

$$\arg A_w = \arg\Pi^{(1)}_{i',w} + \arg\Pi^{(2)}_{i',w} - \arg < \hat{A} >_i, \qquad (14)$$

The argument of the weak value of any three-level observable is the sum of two arguments of weak values of projectors of qubits. Each of these arguments is associated to the solid angle on the Bloch sphere of the triangle spanned by the vectors representing the states $|\phi_i\rangle$, $|\phi_{i'}\rangle$ and $\left|\phi^n_f\right\rangle$,

$$\arg A_w = -\frac{\Omega_{ii'f_1}}{2} - \frac{\Omega_{ii'f_2}}{2} - \arg < \hat{A} >_i \qquad (15)$$

The argument of general observable weak values in 3-level systems has two geometric descriptions, one in CP^2 and a second one on the Bloch sphere. The argument of the weak value of any 3-level observable is a geometric phase associated to the symplectic area in CP^2 of the triangle spanned by the geodesics connecting the three vectors representing the pre-selected state, the application of the observable over the initial state and the post-selected state. Additionally, this symplectic area can be mapped to a Riemannian area on the Bloch sphere thanks to the Majorana description. In this case, the argument of the weak value is the sum of two arguments that are associated to solid angles on the Bloch sphere.

Any weak value can be described using a three-level system, only three vectors are involved in the calculations. In consequence, the results presented in this section are pertinent for the weak value of any N-level observable. The argument of the weak value of any N-level observable is the sum of the argument of the weak value of two qubit projectors (up to a phase of 0 or π). Consequently, in this section we have linked the symplectic area of a triangle in CP^{N-1} to two solid angles on the Bloch sphere. In Fig. 1, we depict the solid angles linked to the argument of the weak value of the controlled NOT gate, essential to produce entangled states in quantum computing,

$$CNOT = \begin{pmatrix} 1 & 0 & 0 & 0 \\ 0 & 1 & 0 & 0 \\ 0 & 0 & 0 & 1 \\ 0 & 0 & 1 & 0 \end{pmatrix}. \qquad (16)$$

In Fig. 1a), we represent the three solid angles on the Bloch sphere in the Majorana representation and the three states involved in the weak value. Nevertheless, one can always reduce the size of the system to a three-level system (independently on the initial vector space size). In Fig. 1b), we depict the two solid angles induced by the argument of the weak value after having reduced the size of the space from 4 levels (requiring 3 states) to 3 levels (involving only 2 states). In Fig. 1c), the geodesic triangle between the three involved vectors is represented in CP^2. To do so, we use the spherical octant projection. Each point of the octant is associated to a torus formed by the two phase components of the Hilbert space, χ_1 and χ_2, $|\psi\rangle = \left(|\psi_0|, e^{j\chi_1}|\psi_1|, e^{j\chi_2}|\psi_2|\right)^T$ [56]. The state $|\psi\rangle$ is projected to the real point $\vec{q} = (|\psi_1|, |\psi_2|, |\psi_0|)$. We also depicted the geodesics between each pair of states in three dimensions. The symplectic area is a contour integral along these geodesics, but it cannot be directly represented. The geodesics in CP^2 do not correspond to great circles on the sphere S^7. Moreover, after applying the Majorana representation to the geodesic, it does not correspond to great circles on the Bloch sphere. Between separable states, geodesics correspond to circular segments on the Bloch sphere [57]. However, they can have very complicated shapes when it comes to not separable states.

WEAK VALUES OF THREE-LEVEL SYSTEMS: SPIN-1

The spin, describing the intrinsic angular momentum of particles, has a central role in quantum physics. The spin operator depends on the type of particle. The Pauli matrices, the chosen generators of SU (2), describe the spin-1/2 [58]. In the case of spin-1, the operators can be described in terms of generators of SU (3). The spin operators along the three different axes are detailed in terms of the Gell-Mann matrices as, $\hat{S}_x = \frac{1}{\sqrt{2}}\left(\hat{\lambda}_1 + \hat{\lambda}_6\right)$, $\hat{S}_y = \frac{1}{\sqrt{2}}\left(\hat{\lambda}_2 + \hat{\lambda}_7\right)$, $\hat{S}_z = \frac{1}{2}\left(\hat{\lambda}_3 + \sqrt{3}\hat{\lambda}_8\right)$ [59], where the Gell-Mann matrices are defined in Appendix 1 and $\hbar = 1$. In several experiments, the weak value of the spin operators has a central role [5, 60]. The real and imaginary parts of the weak values of spin-1/2 operators have been theoretically studied, along with their modulus and argument [5, 36, 61, 62]. As the spin direction can be represented directly on the Bloch sphere, the situation is easy to visualize. However, the weak values of the spin-1 operators were much less studied, specially from a geometrical point of view. One possible method is its study in terms of vectors in CP^2, with a generalization of the Bloch sphere [37]. Here, we focus on the description of weak value of the spin-1 operator on the Bloch sphere using the Majorana formalism introduced in the previous sections.

Let's consider the weak value of a linear combination of the three components of the spin, $\vec{\hat{S}} = n_x\hat{S}_x + n_y\hat{S}_y + n_z\hat{S}_z$. Without loss of generality, by setting an appropriate reference point, we rotate the direction $\vec{n} = (n_x, n_y, n_z)^T$ into $\vec{n} = (0, 0, 1)$. In consequence, we focus on the study of the weak value of $\hat{S}_z$, $S_{z\,w}$. The general pre- and post-selected states have 4 independent parameters each. To simplify the studied case, the pre-

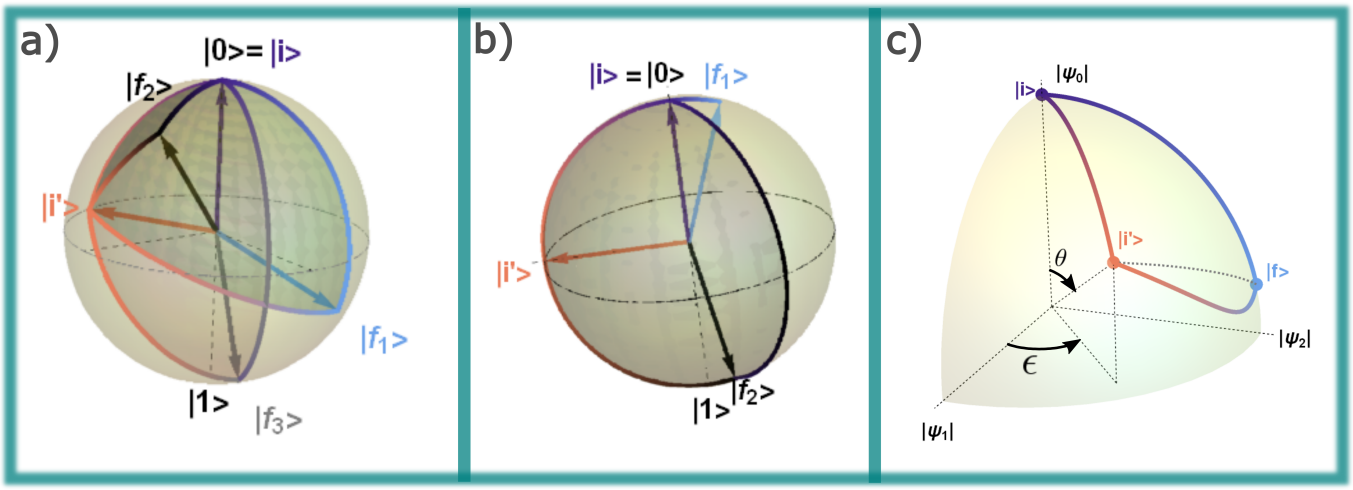

FIG. 1. Representation of the argument of the weak value of the CNOT gate. The pre-selected state is $|\psi_i\rangle = \frac{1}{\sqrt{4}}(1,-j,1,-j)^T$ and the post-selected state is $|\psi_f\rangle = \frac{1}{\sqrt{5}}(1,0,-2,0)^T$. a) Representation of the three solid angles involved in $\arg(CNOT_w)$ on the Bloch sphere. b) Representation of two solid angles concerning the argument of the weak value of the $CNOT$ gate in the reduced approach (three-level system). c) Depiction of the geodesic triangle in the complex projective space CP^2 between the initial state, the application of the CNOT gate over the initial state and the post-selected state, using the spherical octant projection.

selected state is chosen to be $|\psi_i\rangle = \frac{1}{\sqrt{6}}(2,1,j)^T$, where we set the parameters in Eq.(8) to $\epsilon_i = \frac{\pi}{4}$, $\chi_{1i} = 0$, $\chi_{2i} = \frac{3\pi}{2}$, and $\theta = \arccos\sqrt{\frac{2}{3}}$, a simple state, but not a trivial one. In the case of the post-selected state, only two parameters are fixed, $\epsilon_f = \frac{\pi}{4}$, and $\chi_{2f} = 0$, $|\psi_f\rangle = \left(\cos\theta, \frac{1}{\sqrt{2}}\sin\theta e^{j\xi}, \frac{1}{\sqrt{2}}\sin\theta\right)^T$. These states provide a system with two independent parameters, θ and ξ, to study. The application of the spin operator to the pre-selected state is $|\psi_{i'}\rangle = \frac{1}{\sqrt{5}}(2,0,-j)$. Applying the appropriate unitary operators, the initial state is moved to $|\psi_i''\rangle = (1,0,0) \rightarrow |\Psi_i\rangle = |0\rangle|0\rangle$ and the state $|\psi_{i'}\rangle$ to $|\psi_{i'}''\rangle = \left(\sqrt{\frac{3}{10}}, \sqrt{-\frac{3}{5}+\sqrt{\frac{6}{5}}}, 1-\sqrt{\frac{3}{10}}\right)^T \rightarrow |\Psi_{i'}\rangle = |\phi_{i'}\rangle|\phi_{i'}\rangle$, where $|\phi_{i'}\rangle = \left(\left(\frac{3}{10}\right)^{\frac{1}{4}}, \sqrt{1-\sqrt{\frac{3}{10}}}\right)^T$. Making use of these states and applying the Majorana representation to the post-selected state (in Eq.(3) one finds the Majorana polynomial that should be solved), we study the argument of the weak value of the spin-1 as the sum of two arguments of two-level projectors that are associated to two solid angles on the Bloch sphere.

One of the most useful characteristics of weak values is their ability to amplify minute phenomena thanks to their unbounded property. Identifying the behavior of the argument of the weak value when the absolute value tends to infinity is essential due to both the discontinuities that appear in that range and their usefulness.
We study the weak value of $\hat{S}_z$, as a function of a family of post-selected sates described by the parameters θ and ξ. In Fig.(2), we represent the maximum value of the modulus of the weak value of $\hat{S}_z$ for each value of ξ. The maximum of the modulus of the weak values takes place for a determined $\theta_{\max}(\xi)$. We use this value to plot the argument of the weak value at $\theta_{\max}(\xi)$ in terms of ξ. We also depict the angle between the two stars on the Bloch sphere representing the post-selected state, $\vec{f}_1$ and $\vec{f}_2$ at $\theta_{\max}(\xi)$ as a function of ξ. The angle between the two vectors on the Bloch sphere represents an en-

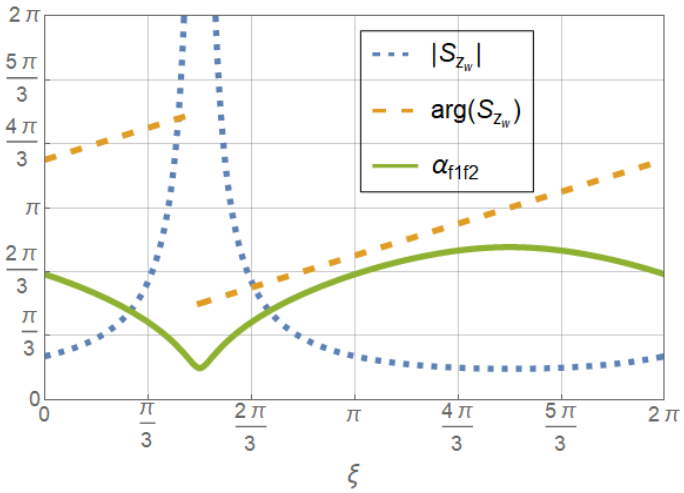

FIG. 2. Representation of the maximum value of the modulus of the weak value for each value of ξ (blue), of the argument of the weak value for the value of $\theta_{max}(\xi)$ at the maximum of the modulus in terms of ξ (green) and of the angle between $\vec{f}_1$ and $\vec{f}_2$ at $\theta_{\max}(\xi)$ as a function of ξ (orange).

tanglement measurement of the two-qubit state. If the angle between the vectors is 0°, the state is separable and thus the entropy of entanglement is 0. On the opposite side, if the angle between the two vectors is 180°, the state is a maximally entangled Bell state. The modulus of the weak value presents a vertical asymptote at $\xi = \frac{\pi}{2}$ because the initial and final states are then orthogonal. At the divergence point, the argument of the weak value presents a π jump. This behavior is typical of the argument of the weak value when there is a divergence in the modulus [26].

The two vectors on the Bloch sphere associated to the final state, $\vec{f}_1$ and $\vec{f}_2$, are the closest, 29.42°, where the maximum value of the modulus tends to infinity. Both the initial state and the application of the operator over the initial state present an entropy of entanglement equal to 0, as the states are separable. Hence, the angle between $\vec{f}_1$ and $\vec{f}_2$ represents the total entanglement of the system.

Having a minimum of entropy of entanglement at the divergence in the modulus of the weak values is counter-intuitive at first. Anomalous weak values are a proof of contextuality [2], a characteristic of non-classicality. Therefore, it could have been expected to find a maximum in the entanglement, which is also a characteristic of non-classicality, at the most anomalous weak value (divergence). To clarify if this is an intrinsic characteristic of the system, we depict the value of the angle between the vectors $\vec{f}_1$ and $\vec{f}_2$ for all values of θ and ξ in Fig. 3. We also include the value of θ at the maximum of the modulus of the weak value, $\theta_{\max}(\xi)$ (red line). We plot the same line for the minimum of the weak value $\theta_{\min}(\xi)$ (green line). There are two absolute minima of the entropy of entanglement. None of them is at the maximum of the modulus of the weak value (red line in the plot). However, the maximum of modulus of the weak value is always located close to the minimum of the entanglement, as it follows the bottom of the valley of minimal entanglement on Fig.3 (slightly to the left). A very similar correlation links the minimum of the modulus of the weak value (green line) and the maximum of the entanglement. The trends are very similar, but slightly shifted. This behavior is very intriguing due to the correlation of the anomalous weak values and non-classicality. We think this should be explored further in the future. The weak value diverges for $\xi = \frac{\pi}{2}, \theta = \frac{\pi}{2}$, as it can been seen in Fig. 2. In Fig. 4 and Fig. 5, we depict the evolution of the argument of the weak value in the Majorana representation in terms of ξ (a), the representation on the Bloch sphere of the solid angles associated to the argument of the weak value for the maximum of the modulus of the weak value (b), and the evolution of the angles on the Bloch sphere as a function of ξ (c). In Fig. 4, we represent a case with θ smaller than at the divergence ($\theta = \frac{\pi}{2} - 0.2$) and in Fig. 5, a case very near the asymptote, ($\theta = \frac{\pi}{2} - 10^{-11}$).

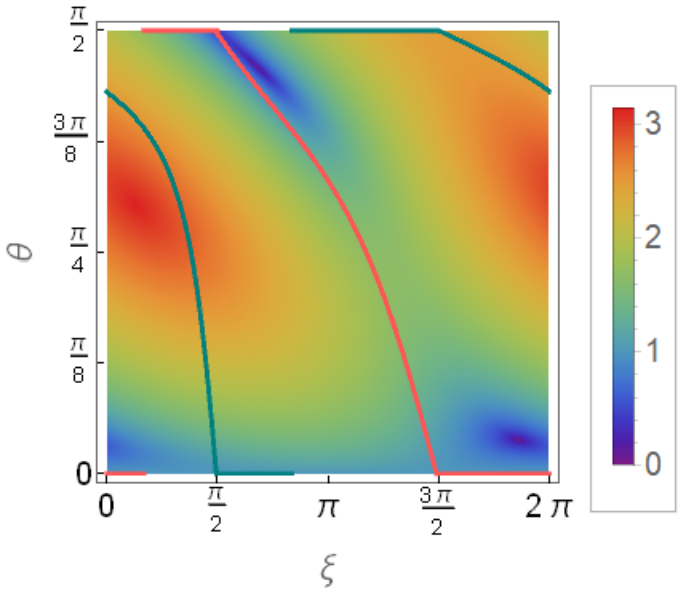

FIG. 3. Color map of of the angle between the vectors representing the post-selected state on the Bloch sphere $\vec{f}_1$ and $\vec{f}_2$ as a function of θ and ξ. The red line represents the angle θ for which the modulus of the weak value is maximum for fixed values of ξ, $\theta_{\max}(\xi)$. The green line represents the angle θ for which the modulus of the weak value is minimum for fixed values of ξ, $\theta_{\min}(\xi)$.

In Fig. 4a), one can perceive that, around $\theta = \frac{\pi}{2}$, the slope of the function is quite big. The closer the θ is from the divergence case, the larger the slope. In Fig. 5a), we represent the extreme case, when $\theta = \frac{\pi}{2}$. There, the slope is infinite, as the argument presents a π jump. In the first case, Fig. 4, the big slope in the argument of the weak value occurs when $\arg\Pi^{(2)}_{i',w}$ passes by 0, so that there is no discontinuity. The other projector presents an argument of the weak value that also has a smooth variation at that point. However, $\arg\Pi^{(1)}_{i',w}$ passes by 0 at $\xi = \frac{3\pi}{2}$. In the second case, Fig. 5, the argument varies linearly with ξ, except at the point of the maximum of the modulus of the weak value, where it exhibits a π jump. This jump is associated to a π jump in the argument of the weak value of the second projector, $\arg\Pi^{(2)}_{i',w}$. This jump is natural, as the vector is passing by the pole of the Bloch sphere. To observe a smooth movement of the star on the Bloch sphere (without change of sense of the movement), a π jump should be present in the function of azimuthal angle, ϕ. The argument of $\Pi^{(2)}_{i',w}$ also passes by 0 at $\xi = \frac{3\pi}{2}$. It appears that the non-smooth behavior of the argument of the weak value induces a non-smooth behavior in one argument of the weak value of a projector in the Majorana representation, while the other argument keeps a smooth behavior.

In figures b) of Fig. 4 and Fig. 5, we represent the solid angles on the Bloch sphere associated to the ar-

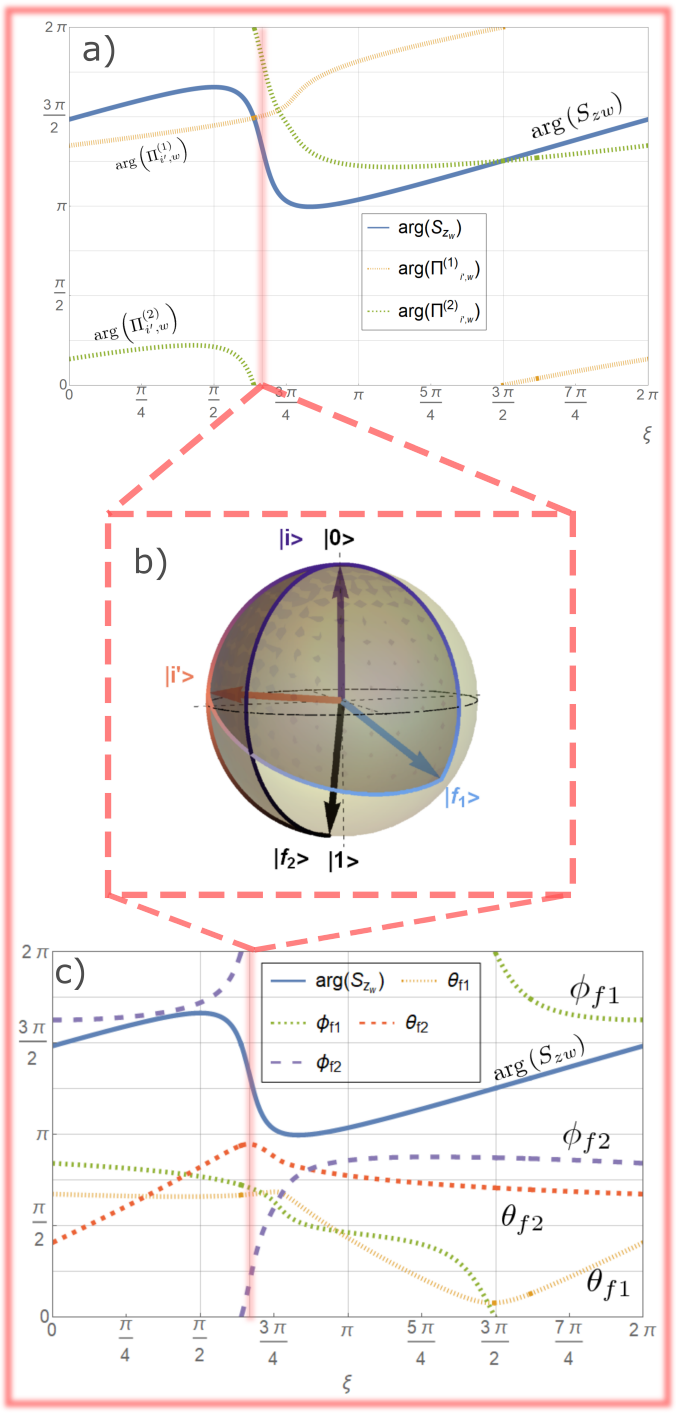

FIG. 4. a) Argument of the weak value of the spin operator, S_{zw}, in terms of ξ, argument of the weak value $\Pi^{(1)}_{i',w}$ and $\Pi^{(2)}_{i',w}$ in terms of ξ for $\theta = \frac{\pi}{2} - 0.2$. b) Solid angles on the Bloch sphere $\Omega_{ii'f_1}$ and $\Omega_{ii'f_2}$ for $\theta = \frac{\pi}{2} - 0.2$ and $\xi = 2.09$. c) Argument of the weak value of $\hat{S}_z$ and polar and azimuthal angles, θ and ϕ, of the vectors representing the post-selected state on the Bloch sphere for $\theta = \frac{\pi}{2} - 0.2$, in terms of ξ. A vertical line has been added in a) and c) at the value of ξ for which the modulus of the weak value is maximum, $\xi = 2.09$.

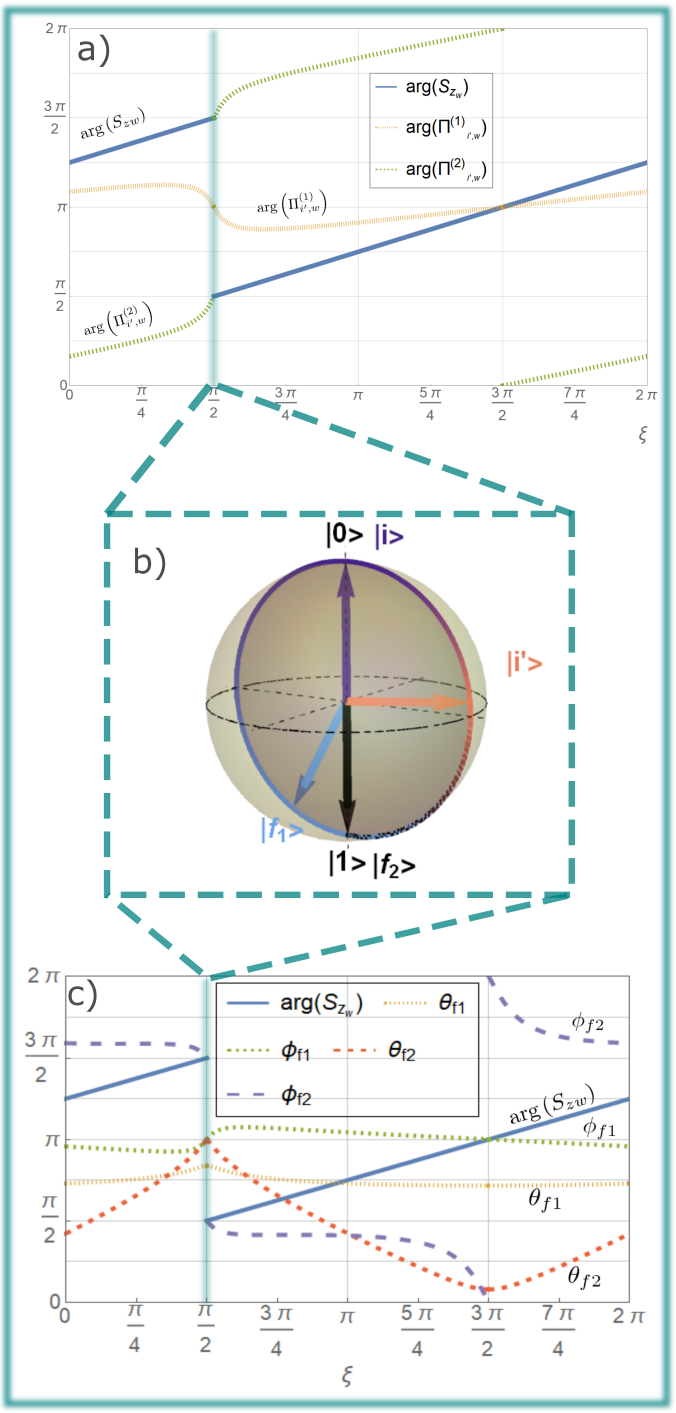

FIG. 5. a) Argument of the weak value of of the spin operator, S_{zw}, in terms of ξ, argument of the weak value $\Pi^{(1)}_{i',w}$ and $\Pi^{(2)}_{i',w}$ in terms ξ with $\theta = \frac{\pi}{2} - 10^{-11}$. b) Solid angles on the Bloch sphere $\Omega_{ii'f_1}$ and $\Omega_{ii'f_2}$ for $\xi = \frac{\pi}{2}$ and $\theta = \frac{\pi}{2}$. c) Argument of the weak value of $\hat{S}_z$ and polar and azimuthal angles, θ and ϕ, of the vectors representing the post-selected state on the Bloch sphere for $\theta = \frac{\pi}{2}$, in terms of ξ. A vertical line has been added in a) and c) at the value of ξ for which the modulus of the weak value is maximum, $\xi = \frac{\pi}{2}$.

gument of the weak value. In each figure, the solid angles correspond to the case in which the modulus of the weak value is maximum, $\{\theta = \pi/2 - 0.2, \xi = 2.09\}$ and $\{\theta = \frac{\pi}{2}, \xi = \frac{\pi}{2}\}$ respectively. The value of the maximum is highlighted with a vertical line (pink in Fig. 4 and green in Fig. 5). Far from the divergence, Fig. 4, there are clearly two solid angles. However, very close to the divergence, Fig. 5, all the vectors are nearly on the same plane on the Bloch sphere. One of the qubit states representing the post-selected state in the Majorana representation is orthogonal to the qubit state representing the initial state, a condition required for the appearance of a divergence. All vectors on the Bloch sphere are not necessarily on the same plane when a divergence is present. When the initial and final states are orthogonal, the great circle between $\vec{i}$ and $\vec{f}_2$ is not unique as there are different paths with the same distance. At $\theta = \frac{\pi}{2}$, in Fig. 5, the vectors $\vec{f}_1$ and $\vec{f}_2$ are the closest and thus the entanglement between them is the minimum.

In Fig. 4c, 5c, we depict both the azimuthal and the polar angles of the two qubits representing the final state, at the divergence position, $\theta = \frac{\pi}{2}$ in Fig. 5 and at a smaller value of θ, Fig. 4. In Fig. 4c, the polar angle θ_1 is approximately constant from $\xi = 0$ until the maximum of the modulus of the weak value (vertical line), $\xi = 2.09$. The maximum occurs at a value a bit larger than $\xi = 2.09$. Then, it decreases, presenting a minimum at $\xi = \frac{3\pi}{2}$, where the azimuthal angle, ϕ_1, passes by 0. After that point, the polar angle increases until reaching the initial value. At the jump position, in Fig. 5. The polar angle of one of the qubits, θ_2, representing the post-selected state has a maximum at the position of the maximum of the modulus of the weak value (vertical line), where it is orthogonal to the pre-selected state, $\langle f_2|i\rangle = 0$. The polar angle of the other qubit, θ_1, is almost constant in terms of ξ for $\theta = \frac{\pi}{2}$. It exhibits a smooth maximum at $\xi = \frac{\pi}{2}$. At this point the two polar angles are the closest. In Fig. 4c, ϕ_2 has a large slope near the maximum of the modulus, similarly to the argument of the weak value. In Fig. 5c, ϕ_2 has a π jump at $\xi = \frac{\pi}{2}$, where the divergence takes place. It also presents a large slope when the argument of the weak value passes by π, when the weak value is purely real. It appears that the azimuthal angle presents a similar behavior as the argument of the weak value when a non-smooth behavior appears.

Using the Majorana representation, we studied different aspects of the weak values, such as the entropy of entanglement. We noticed that an interesting behavior occurs: a maximum (minimum) of the entanglement is near a minimum (maximum) of the modulus of the weak value. Only the Majorana approach allows this analysis. Simply visualizing the behavior of the qubits representing the different states on the Bloch sphere, we can interpret the evolution of the argument of the weak value.

CONCLUSIONS

We applied the Majorana symmetric representation to study the geometry of the argument of weak values of N-level general observables on the Bloch sphere. The weak value of any observable is proportional to the weak value of an effective projector that is defined as the normalized application of the observable over the pre-selected state. The constant of proportionality is real. Hence, the argument of the weak value of any observable is the argument of the weak value of a projector modulo π.

The modulus of the weak value of a general observable is the product of $N-1$ moduli of weak values of projectors in CP^1 and constants that are independent on the post-selected state. The argument of the weak value of any observable is the sum of $N-1$ arguments of 2-level systems, plus a phase that is either 0 or π. Each of these arguments represents a solid angle on the Bloch sphere.

Any weak value depends only on three states. Thus, applying different unitary operators, it is possible to map these states to a three-level system, giving a special importance to the qutrit case. Doing so, we map a symplectic area in CP^{N-1} to a sum of two solid angles, instead of $N-1$, on the Bloch sphere (up to a constant that is either 0 or π). The solid angles on the Bloch sphere are determined by the great circles between the four qubit vectors (the two degenerate states associated to the initial state, the two degenerate states linked to the observable, and the two entangled states describing the final state). However, these great circles are not geodesics between the states in CP^{N-1}.

We applied these results to the spin-1 operator for anomalous weak values in the region of weak value amplification. Using a specific case, we studied the argument of the weak value when the modulus tends to infinite (asymptotic behavior). We found that when the weak value diverges, the angle between the two vectors representing the post-selected state on the Bloch sphere presents a constrained minimum. The angle between the two qubits representing the post-selected state on the Bloch sphere gives a measure of the total entanglement of the system. The maximum value of the modulus is for any value of the angle ξ near the minimum of entanglement. The non-smooth behavior of the argument of the weak value seems to be associated to the evolution of the azimuthal angle of the qubits on the Bloch sphere. The azimuthal angle controls the phase of the qubit state components. Ultimately, it is thus responsible for any phase appearing in the qubit weak value.

APPENDIX 1

The order of the Gell-Mann matrices used in this paper is,

$$\hat{\lambda}_1 = \begin{pmatrix} 0 & 1 & 0 \\ 1 & 0 & 0 \\ 0 & 0 & 0 \end{pmatrix} \qquad \hat{\lambda}_2 = \begin{pmatrix} 0 & -i & 0 \\ i & 0 & 0 \\ 0 & 0 & 0 \end{pmatrix} \tag{17}$$

$$\hat{\lambda}_3 = \begin{pmatrix} 1 & 0 & 0 \\ 0 & -1 & 0 \\ 0 & 0 & 0 \end{pmatrix} \qquad \hat{\lambda}_4 = \begin{pmatrix} 0 & 0 & 1 \\ 0 & 0 & 0 \\ 1 & 0 & 0 \end{pmatrix}$$

$$\hat{\lambda}_5 = \begin{pmatrix} 0 & 0 & -i \\ 0 & 0 & 0 \\ i & 0 & 0 \end{pmatrix} \qquad \hat{\lambda}_6 = \begin{pmatrix} 0 & 0 & 0 \\ 0 & 0 & 1 \\ 0 & 1 & 0 \end{pmatrix}$$

$$\hat{\lambda}_7 = \begin{pmatrix} 0 & 0 & 0 \\ 0 & 0 & -i \\ 0 & i & 0 \end{pmatrix} \qquad \hat{\lambda}_8 = \frac{1}{\sqrt{3}} \begin{pmatrix} 1 & 0 & 0 \\ 0 & 1 & 0 \\ 0 & 0 & -2 \end{pmatrix}$$

APPENDIX 2

In this paper, we used the symmetric Majorana representation of CP^N, which should not be confused with the Majorana representation of spinors. The representation maps N-level quantum states to $N-1$ stars on the Bloch sphere. To do so, it associates the basis of N-level systems with the symmetric tensorial products of two-level states [50].

Let's consider a four-level system. The basis is formed by the states $|0\rangle$, $|1\rangle$, $|2\rangle$, $|3\rangle$. The Majorana representation associates the states as follows,

$$\begin{aligned} |0\rangle &\to |\Psi\rangle = |0\rangle\,|0\rangle\,|0\rangle \\ |1\rangle &\to |\Psi\rangle = \frac{1}{\sqrt{3}}\left(|1\rangle\,|0\rangle\,|0\rangle + |0\rangle\,|1\rangle\,|0\rangle + |0\rangle\,|0\rangle\,|1\rangle\right) \\ |2\rangle &\to |\Psi\rangle = \frac{1}{\sqrt{3}}\left(|1\rangle\,|1\rangle\,|0\rangle + |1\rangle\,|0\rangle\,|1\rangle + |0\rangle\,|1\rangle\,|1\rangle\right) \\ |3\rangle &\to |\Psi\rangle = |1\rangle\,|1\rangle\,|1\rangle \end{aligned} \tag{18}$$

where the order of the basis can be chosen. This association is straightforwardly generalized to N-level systems,

$$\begin{aligned} |0\rangle &\to |\Psi\rangle = \underbrace{|0\rangle\,|0\rangle\,....\,|0\rangle}_{N-1} \\ |1\rangle &\to |\Psi\rangle = \frac{1}{\sqrt{N-1}} \sum_P |1\rangle\,\underbrace{|0\rangle\,|0\rangle\,...\,|0\rangle}_{N-2} \\ &\vdots \\ |N-2\rangle &\to |\Psi\rangle = \frac{1}{\sqrt{N-1}} \sum_P |0\rangle\,\underbrace{|1\rangle\,|1\rangle\,...\,|1\rangle}_{N-2}, \\ |N-1\rangle &\to |\Psi\rangle = \underbrace{|1\rangle\,|1\rangle\,...\,|1\rangle}_{N-1}, \end{aligned} \tag{19}$$

where P runs through all the permutations of the states $|0\rangle$ and $|1\rangle$. In general, it is possible to calculate the Majorana stars of any general N-level state using the polynomial of Eq.(3).

REFERENCES

* lorena.ballesteros@unamur.be, yves.caudano@unamur.be

[1] D. J. Starling, P. B. Dixon, A. N. Jordan, and J. C. Howell, Phys. Rev. A **82**, 063822 (2010).
[2] M. F. Pusey, Phys. Rev. Lett. **113**, 200401 (2014).
[3] J. Dressel and A. N. Jordan, Phys. Rev. Lett. **109**, 230402 (2012).
[4] P. A. Mello, in *AIP Conf. Proc.*, Vol. 1575 (American Institute of Physics, 2014) pp. 136–165.
[5] Y. Aharonov, D. Z. Albert, and L. Vaidman, Phys. Rev. Lett. **60**, 1351 (1988).
[6] B. E. Svensson, Quanta **2**, 18 (2013).
[7] R. Jozsa, Phys. Rev. A **76**, 044103 (2007).
[8] H. Wiseman, Phys. Rev. A **65**, 032111 (2002).
[9] K. Ogawa, H. Kobayashi, and A. Tomita, Phys. Rev. A **101**, 042117 (2020).
[10] F. De Zela, Phys. Rev. A **105**, 042202 (2022).
[11] P. B. Dixon, D. J. Starling, A. N. Jordan, and J. C. Howell, Phys. Rev. Lett. **102**, 173601 (2009).
[12] G. B. Alves, B. Escher, R. de Matos Filho, N. Zagury, and L. Davidovich, Phys. Rev. A **91**, 062107 (2015).
[13] L. Xu, Z. Liu, A. Datta, G. C. Knee, J. S. Lundeen, Y.-q. Lu, and L. Zhang, Phys. Rev. Lett. **125**, 080501 (2020).
[14] O. Zilberberg, A. Romito, and Y. Gefen, Phys. Rev. Lett. **106**, 080405 (2011).
[15] L. Luo, X. Qiu, L. Xie, X. Liu, Z. Li, Z. Zhang, and J. Du, Opt. Express **25**, 21107 (2017).
[16] A. N. Jordan, P. Lewalle, J. Tollaksen, and J. C. Howell, Quantum Stud.: Math. Found. **6**, 169 (2019).
[17] H. F. Hofmann, Phys. Rev. A **81**, 012103 (2010).
[18] J. S. Lundeen and C. Bamber, Phys. Rev. Lett. **108**, 070402 (2012).
[19] Y. Kim, Y.-S. Kim, S.-Y. Lee, S.-W. Han, S. Moon, Y.-H. Kim, and Y.-W. Cho, Nat. Commun. **9**, 1 (2018).
[20] X. Zhu and Q. Wei, Ann. Phys. **376**, 283 (2017).
[21] J. S. Lundeen, B. Sutherland, A. Patel, C. Stewart, and C. Bamber, Nature **474**, 188 (2011).
[22] A. K. Pati, U. Singh, and U. Sinha, Phys. Rev. A **92**, 052120 (2015).
[23] A. Lund, New J. Phys. **13**, 053024 (2011).
[24] S. Tamate, H. Kobayashi, T. Nakanishi, K. Sugiyama, and M. Kitano, New J. Phys. **11**, 093025 (2009).
[25] Y. Kedem and L. Vaidman, Phys. Rev. Lett. **105**, 230401 (2010).
[26] M. Cormann and Y. Caudano, J. Phys. A Math. Theor. **50**, 305302 (2017).
[27] L. B. Ho and N. Imoto, J Math Phys. **59**, 042107 (2018).
[28] C. Samlan and N. K. Viswanathan, J Opt. **19**, 125401 (2017).

[29] M. Pal, S. Saha, B. Athira, S. D. Gupta, and N. Ghosh, Phys. Rev. A **99**, 032123 (2019).
[30] Y.-W. Cho, Y. Kim, Y.-H. Choi, Y.-S. Kim, S.-W. Han, S.-Y. Lee, S. Moon, and Y.-H. Kim, Nat. Phys. **15**, 665 (2019).
[31] R. Kunjwal, M. Lostaglio, and M. F. Pusey, Phys. Rev. A **100**, 042116 (2019).
[32] M. J. Hall, Phys. Rev. A **69**, 052113 (2004).
[33] J. Dressel, Phys. Rev. A **91**, 032116 (2015).
[34] J. Dressel and A. N. Jordan, Phys. Rev. A **85**, 012107 (2012).
[35] H. F. Hofmann, Phys. Rev. A **83**, 022106 (2011).
[36] M. Cormann, M. Remy, B. Kolaric, and Y. Caudano, Phys. Rev. A **93**, 042124 (2016).
[37] L. Ballesteros Ferraz, D. L. Lambert, and Y. Caudano, Quantum Sci. Technol. **7** (2022).
[38] E. Majorana, Il Nuovo Cimento (1924-1942) **9**, 43 (1932).
[39] J. Hannay, J. Phys. A: Math. Gen. **31**, L53 (1998).
[40] K. Y. Bliokh, M. A. Alonso, and M. R. Dennis, Rep. Prog. Phys. **82**, 122401 (2019).
[41] D. J. Markham, Phys. Rev. A **83**, 042332 (2011).
[42] J. Zimba, Electron. J. Theor. Phys. **3**, 143 (2006).
[43] D. M. Galindo and J. A. Maytorena, Physical Review A **105**, 012601 (2022).
[44] K. Akhilesh, B. Divyamani, A. Usha Devi, K. Mallesh, *et al.*, Quant. Inform. Process. **18**, 1 (2019).
[45] J. G. Kirkwood, Phys. Rev. **44**, 31 (1933).
[46] E. M. Rabei, N. Mukunda, R. Simon, *et al.*, Phys. Rev. A **60**, 3397 (1999).
[47] S. Tamate, K. Ogawa, and M. Kitano, Phys. Rev. A **84**, 052114 (2011).
[48] As the expressions of the weak value only depend on the projector, $\hat{\Pi}_{i'}$, this phase has no impact.
[49] F. Bloch and I. I. Rabi, Rev. Mod. Phys. **17**, 237 (1945).
[50] A. Devi, A. Rajagopal, *et al.*, Quantum Inf. Process. **11**, 685 (2012).
[51] R. A. Bertlmann and P. Krammer, J. Phys. A Math. Theor. **41**, 235303 (2008).
[52] A. Andreev, O. Shoutova, S. Trushin, and S. Y. Stremoukhov, J Opt. Soc. Am. B **39**, 1775 (2022).
[53] T. Ravon and L. Vaidman, J. Phys. A Math. Theor. **40**, 2873 (2007).
[54] A. Acin, T. Durt, N. Gisin, and J. I. Latorre, Phys. Rev. A **65**, 052325 (2002).
[55] As the expressions of the weak value depend on the projector, $\Pi_{i'}$, this phase has no impact.
[56] K. Mallesh, N. Mukunda, *et al.*, J. Phys. A: Math. Gen. **30**, 2417 (1997).
[57] V. Mittal, S. K. Goyal, *et al.*, Phys. Rev. A **105**, 052219 (2022).
[58] R. Eisberg and R. Resnick, *Quantum physics of atoms, molecules, solids, nuclei, and particles* (1985).
[59] S. Binicioğlu, M. A. Can, A. A. Klyachko, and A. S. Shumovsky, Found. Phys. **37**, 1253 (2007).
[60] A. Romito, Y. Gefen, and Y. M. Blanter, Phys. Rev. Lett. **100**, 056801 (2008).
[61] I. Duck, P. M. Stevenson, and E. Sudarshan, Phys. Rev. D **40**, 2112 (1989).
[62] E. Sjöqvist, Phys. Lett. A **359**, 187 (2006).